

A MULTI-BAND PHOTOMETRIC STUDY OF TIDAL DEBRIS
IN A COMPACT GROUP OF GALAXIES: SEYFERT'S SEXTET

SHINGO NISHIURA¹, YASUHIRO SHIOYA², TAKASHI MURAYAMA^{2,3,4}, YASUNORI SATO^{4,5}, TOHRU
NAGAO^{2,4}, YOSHIAKI TANIGUCHI^{2,4}, & D. B. SANDERS⁶

¹Kiso Observatory, Institute of Astronomy, The University of Tokyo, Mitake-mura, Kiso-gun, Nagano
397-0101, Japan

²Astronomical Institute, Graduate School of Science, Tohoku University, Aramaki, Aoba, Sendai 980-8578,
Japan

³Visiting astronomer of Kiso Observatory, University of Tokyo, Japan

⁴Visiting astronomer of Mauna Kea Observatories, University of Hawaii, USA

⁵Institute of Astronomy, The University of Tokyo, 2-21-1, Osawa, Mitaka, Tokyo 181-0015, Japan

⁶Institute for Astronomy, University of Hawaii, 2680 Woodlawn Drive, Honolulu, HI 96822, USA

PASJ: *Publ. Astron. Soc. Japan* 54, No. 1, in press.

ABSTRACT

In order to investigate the properties of the prominent tidal debris feature extending to the northeast of the compact group of galaxies Seyfert's Sextet, we analyzed multi-band (U , B , V , VR , R , I , J , H and K') photometric imaging data and obtained the following results: 1) The radial surface brightness distribution of this tidal debris in Seyfert's Sextet (TDSS) in each band appears to be well approximated by an exponential profile. 2) The observed $B - V$ color of TDSS is similar to those of dwarf elliptical galaxies in nearby clusters. 3) Comparing the spectral energy distribution (SED) of TDSS with theoretical photometric evolution models and with the SED of the stars in the outer part of HCG 79b, we find that its SED is comparable to that of a ~ 10 Gyr-old stellar population with solar metallicity, similar to the stellar population in the outer part of HCG 79b. This suggests that TDSS consists of stars that may have been liberated from HCG 79b by strong galaxy interactions, not a pre-existing dwarf galaxy previously thought.

Subject headings: galaxies:individual (Seyfert's Sextet) - galaxies: formation - galaxies:interactions - galaxies:structure

1. INTRODUCTION

Although dwarf galaxies are the most numerous extragalactic objects in the nearby Universe (e.g., Ferguson & Binggeli 1994; Binggeli, Sandage & Tammann 1988; Mateo 1998), it seems unclear how they are related in origin to typical large (i.e., L^*) galaxies. Dwarf galaxies could be formed through the same formation mechanism as that of large galaxies; e.g., gravitational collapse of protogalactic gas clouds (Dekel & Silk 1986; White & Frenk 1991; Frenk et al. 1996; Kauffmann, Nusser & Steinmetz 1997). However, it is known that dwarf elliptical galaxies (dEs) apparently belong to a different class from normal large ellipticals (Es) in the fundamental plane (e.g., Kormendy 1985), suggesting that the formation and/or evolution processes of dwarfs may not always be the same as those of larger ellipticals.

It has been argued from an observational view point that dwarf galaxies may be formed by galaxy collisions because there appears to be morphological evidence for dwarf galaxies in the tidal tails of interacting galaxies (Zwicky 1956; Schweizer 1978; Duc et al. 2000); i.e., gas-rich dwarf irregular galaxies, can be made out of stellar and gaseous material pulled out into intergalactic space by tidal forces from the disks of colliding parent galaxies. This possibility has been recently reinforced by a number of pieces of observational evidence (Schweizer 1982; Bergvall & Johansson 1985; Schombert, Wallin & Struck-Marcell 1990; Mirabel, Lutz & Maza 1991; Mirabel, Dottori & Lutz 1992; Duc & Mirabel 1994, 1998; Duc et al.

2000; Yoshida, Taniguchi & Murayama 1994; Braine et al. 2000; Weilbacher et al. 2000). Also, Hunsberger et al. (1996; 1998) find an excess of dwarf galaxies in compact groups of galaxies apparently caused by interactions among group members. Such formation of tidal dwarf galaxies (TDGs) has also been demonstrated by numerical simulations of merging/interacting galaxies (Barnes & Hernquist 1992; Elmegreen, Kaufman & Thomasson 1993). Therefore, tidal formation seems to potentially be an important formation mechanism for dwarf galaxies (Okazaki & Taniguchi 2000 and references therein).

One famous tidal debris system extends to the northeast of Seyfert's Sextet (hereafter SS). SS is one of the most famous, as well as densest, compact groups of galaxies (Seyfert 1948a, 1948b; see for a review, Rabaça 1996). This group is also a Hickson compact group (hereafter HCG) of galaxies, HCG 79 (Hickson 1982; 1993). Many subsequent studies of SS have mentioned that the galaxies in SS appear to show morphologically and dynamically peculiar properties (Sulentic & Lorre 1983; Rubin, Hunter, & Ford 1991; Bettoni & Fasano 1993; Mendes de Oliveira & Hickson 1994; Bonfanti et al. 1999; Nishiura et al. 2000a). Hickson himself regarded SS as a galaxy quartet (HCG 79a, 79b, 79c, and 79d). A fifth component, HCG 79e, was found to be a redshift-discordant galaxy that is believed to have no physical relation to SS (Hickson 1992). A sixth object, or more precisely the north-eastern optical fuzz, is now considered likely to be tidal debris associated with the morphologically peculiar galaxy HCG 79b (Ru-

bin et al. 1991; Williams et al. 1991; Mendes de Oliveira & Hickson 1994; Vílchez & Iglesias-Páramo 1998).

Current X-ray observations are not sensitive enough to detect any X-ray emission that may originate from intra-group gas that might be present in SS (Pildis, Bregman, & Evrard 1995; Ponman et al. 1996). However, Sulentic & Lorre (1983) and Nishiura et al. (2000b) detected a faint optical envelope around SS that is plausibly composed of stars tidally liberated from the galaxies in SS, plus Williams, McMahon & van Gorkom (1991) found extended HI emission. These observations suggest that SS is a physically real compact group.

In this paper, we present results of our photometric study of TDSS. Since this tidal debris system in SS (hereafter TDSS) is morphologically similar to other tidal debris, such as Arp 105S and Arp 245N (Braine et al. 2000), we will also compare the photometric properties of TDSS with these two tidal debris. Throughout this paper we adopt a distance to SS of 44 Mpc determined using the mean recession velocity of HCG 79a, 79b, 79c, and 79d referenced to the galactic standard of rest, $V_{\text{GSR}} = 4449 \text{ km s}^{-1}$ (de Vaucouleurs et al. 1991), and a Hubble constant, $H_0 = 100 \text{ km s}^{-1} \text{ Mpc}^{-1}$.

2. DATA

2.1. $F336W$, $F439W$, $F555W$, and $F814W$ images

We obtained the archival HST/WFPC $F439W$ images of SS (PI: Sulentic, J. W.). The total exposure time was 8100 seconds (Wu, Rabaça & Sulentic 1994; Rabaça 1997). We used IRAF¹ to reject cosmic-rays and to combine images.

We also obtained the flux-calibrated archival HST/WFPC2 $F336W$, $F439W$, $F555W$, and $F814W$ images of SS (PI: Hunsberger, S. D.). The total exposure times were 5200 seconds for $F336W$, 5200 seconds for $F439W$, 2000 seconds for $F555W$, and 2000 seconds for $F814W$.

We compute a Johnson B magnitude assuming that the filter function of $F439W$ is the same as that of Johnson B . We also do a Johnson V magnitude assuming that the filter function of $F555W$ is the same as that of Johnson V . According to Fig 11 in Holtzman et al (1995), Johnson $B \sim B(F439W) - 0.1$ for Johnson B - Johnson V of about 1. Johnson $V \sim V(F555W) - 0.05$ for Johnson V - I of about 1. Apparent Johnson B and Johnson V magnitudes of TDSS may be 0.1 and 0.05 mag brighter, respectively. But, our results using $B-V$ and $V-I$ colors do not significantly change.

2.2. V and R images

V - and R -band deep images of SS were obtained with the 1K (1024×1024) CCD camera attached to the 105 cm Schmidt telescope of the University of Tokyo at KISO Observatory, on 20 April, 1996 (R -band) and 21 April, 1996 (V -band). The camera provided a $\approx 12'.5 \times 12'.5$ field of view. The spatial resolution was $0''.75$ per pixel. The integration time for each exposure was set to 900 seconds for V -band and 600 seconds for R -band. Four exposures for the V -band and five exposures for the R -band were taken; thus, the total integration time was 3,600 seconds in the V -

band image and 3,000 seconds in the R -band image. The seeing was $\approx 4''.6$ for V -band and $\approx 5''.2$ for R -band during the observations. Data reduction was performed in a standard way using IRAF. Flux calibration for the R -band images was made using the data of photometric standard stars in the field of PG 0942+029 (Landolt 1992). The V -band observations were carried out under non-photometric conditions. V -band image calibration was performed simply by using the measured magnitude of a star in the same frame of SS, AC2000-738224 (Urban et al. 1997; Kislyuk et al. 1999). The photometric errors were estimated to be ± 0.27 mag for the V -band and ± 0.04 mag for the R -band.

2.3. VR and I images

We used VR - and I -band images taken from our previous studies (Murayama et al. 2000; Nishiura et al. 2000b). Since the VR -band is not a standard photometric band (Jewitt, Luu & Chen 1996), we adopted an AB magnitude scale for this bandpass.

2.4. J and H image

Near-infrared J - and H - images of SS were obtained using the 105 cm Schmidt telescope at the KISO Observatory during the period between 1 July 2001 and 4 July 2001. The telescope was equipped with a large-format near-infrared camera called the Kiso Observatory Near-Infrared Camera (KONIC) (Itoh et al. 1995). KONIC have 1040×1040 pixels providing a $\approx 18' \times 18'$ field of view. The spatial resolution was $1''.06$ arcsec per pixel. We use the images further binned into 520×520 pixels, hence a pixel scale is $2''.12$ per the 2×2 binned pixels.

The integration time for each exposure was set to 180 seconds. Twenty five exposures for J -band and thirty two exposures for H -band were taken. Therefore the total integration times were 4500 seconds for J -band and 5760 seconds for H -band, respectively. The seeing was $\sim 2''.5$ during the observation.

Data reduction was performed in a standard way using IRAF. Flux calibration was made using the measured magnitudes of stars by 2MASS in the same frame of SS, 1558526+203915, 1558546+205049, and 1559287+204805. The photometric errors were estimated to be $\pm 0.0x$ mag for J -band and to be $\pm 0.0x$ mag for H -band, respectively.

2.5. K' image

Near-infrared K' -band images of SS were obtained with the 256×256 Infrared Camera attached to the $f/13.5$ Cassegrain focus of the University of Hawaii 0.6 m Planetary Patrol telescope at Mauna Kea Observatory, on 9 May 1994. The camera provided a $\approx 8'.5 \times 8'.5$ field of view. The spatial resolution was $2''.0$ arcsec per pixel. The integration time for each exposure was set to 120 seconds. Eight exposures were taken; thus, the total integration time amounted to 960 seconds. The seeing was $\sim 2''.4$ during the observation. Data reduction was performed in a standard way using IRAF. Flux calibration was made using the data of the UKIRT bright standard stars HD84800, HD105601, and HD136754, translated into K' -band values (Wainscoat & Cowie 1992). The photometric errors were estimated to be ± 0.08 mag.

All the images of SS and TDSS are shown in Figure 1.

¹Image Reduction and Analysis Facility (IRAF) is distributed by the National Optical Astronomy Observatories, which are operated by the Association of Universities for Research in Astronomy, Inc., under cooperative agreement with the National Science Foundation.

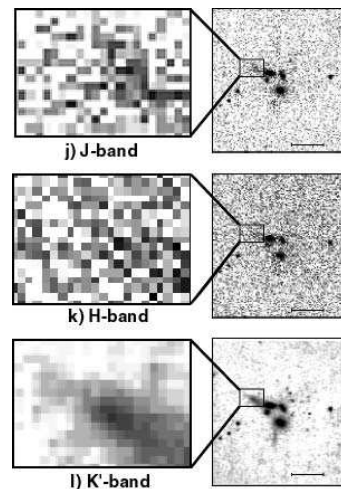
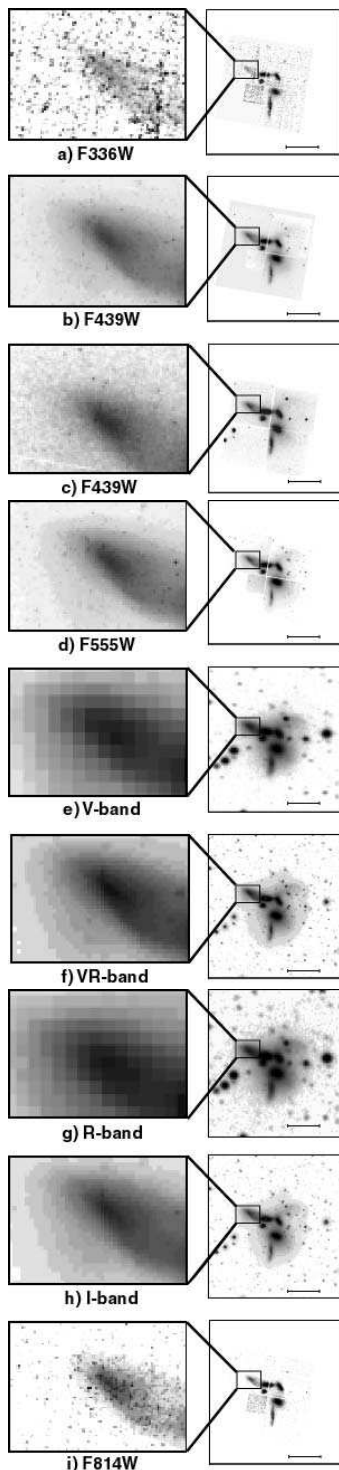


FIG. 1.— The (a) $F336W$, (b) $F439W$, (c) $F439W/WFPC$, (d) $F555W$, (e) V -band, (f) VR -band, (g) R -band, (h) I -band, (i) $F814W$, (j) J -band, (k) H -band and (l) K' images of TDSS and SS before smearing (see text). The horizontal bars correspond to 1 arcmin $\simeq 12.8$ kpc. North is up and east is to the left.

3. RESULTS

3.1. Surface Brightness Profiles of TDSS

Surface photometry of TDSS was carried out using the Surface Photometry Interactive Reduction and Analysis Library (SPIRAL: Hamabe & Ichikawa 1992). The surface brightness profile along the eastern major axis in each passband is shown in Figure 2. Note that the western part of TDSS may suffer from slight contamination by HCG 79b. To minimize light contamination from HCG 79b, we show only the eastern-side profile in Figure 2. In this procedure, the center of TDSS is defined as the peak position in the VR - and I -band images since our deepest exposures are at VR - and I -band. The peak positions of the two images are the same: $\alpha = 15^{\text{h}}57^{\text{m}}03^{\text{s}}.2$, $\delta = +20^{\circ}54'26''.4$ (B1950.0).

Unfortunately, the $F336W$, $F439W$ with $HST/WFPC2$, J - and H -band surface brightness profiles of TDSS are very low signal-to-noise ratio. For surface brightness profiles in the other filter bands, there appears to be a hump at $r \approx 9''$ in the $F555W$, VR -, I - band, and $F814W$ profiles (Figure 2). A broader hump is also seen in the K' -band profile. Since we cannot find any foreground or background object at $r \approx 9''$, these humps are considered to be real. On the other hand, such a hump cannot be seen in the V - and R -band images. However, since these images were obtained in poor seeing conditions, the hump may simply be smeared out. The $F439W$ image with $HST/WFPC$ also appears to be too shallow to detect the hump at $r \approx 9''$. Sulentic & Lorre (1983), Rubin et al. (1991), and Nishiura et al. (2000b) have reported that there is a faint optical envelope around SS presumably formed by strong galaxy collisions. Therefore, this hump might represent the overlap between the faint end of TDSS and the bright end of the faint optical envelope.

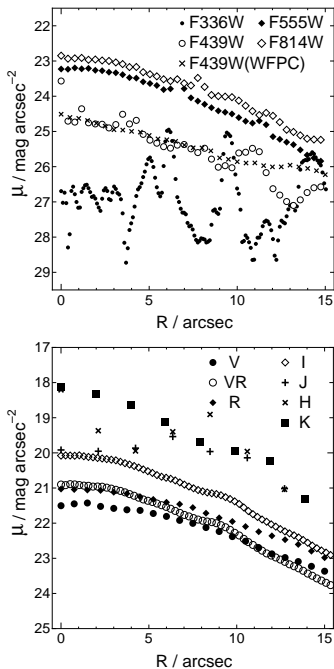


FIG. 2.— The surface brightness (SB) profiles along the major axis of TDSS as functions of distance from the center. (a) Filled circles, filled diamonds, and open diamonds indicate SB profile in $F336W$, $F555W$, and $F814W$, respectively. Open circles mean SB profiles in $F439W$ with $WFPC2$. Crosses represent SB profiles in $F439W$ with $WFPC$. (b) Filled circles, open circles, filled diamonds, and open diamonds mean SB profiles in V -, VR -, R -, I -band. Pluses, crosses, and filled squares indicate SB profiles in J -, H -, and K -band. All of SB profiles are without smearing.

The radial surface brightness profiles in the high-quality VR - and I -band images appear to be well represented by an exponential-like profile. Such profiles are often observed in dwarf elliptical galaxies (Faber & Lin 1983; Ichikawa et al. 1986a; 1986b), and also in the tidal dwarf galaxy Arp 245N (Duc et al. 2000).

3.2. Photometric Properties of TDSS

In order to investigate the stellar content of TDSS, we now investigate its photometric properties. We first smear the $F336W$ -, $F439W$ -, $F555W$ -, V -, VR -, I -, $F814W$ -, K' -band images to match the seeing of our R -band image, given that the R -band image has the largest seeing value in our image set. Since a point spread function (PSF) of KONIC is undesirably extended (Yanagisawa et al. 1996), for the J - and H - images after the PSF deconvolution were carried out with the Lucy-Richardsons method realized in the STSDAS packages, we smear both images to match the seeing of our R -band image. Then, using the GAIA/SKYCAT² package, we integrated the light within an ellipse which encloses TDSS in each band; the semi-major axis = $10''.5$, the eccentricity = 0.90, and the position angle = 46° . The results are shown in Table 1. Unfortunately, in $F336W$ image large noise overlapped with TDSS, we obtained only upper limit of $F336W$ flux of TDSS.

We compare the color-magnitude relation found for TDSS with those of other similar objects by using a $B - V$ versus M_B diagram. We obtain an averaged apparent mag-

nitude of 17.13 ± 0.01 mag (Johnson B) for TDSS after correcting for galactic extinction (de Vaucouleurs et al. 1991; Cardelli et al. 1989; Schlegel et al. 1998). We also obtained apparent Johnson V magnitudes of 16.17 ± 0.27 (observed with 1K-CCD camera) and of 16.40 ± 0.003 mag (observed with $WFPC2$). Thus, we obtained a Johnson $B - V$ colors for TDSS of 0.73 ± 0.01 mag and 0.97 ± 0.27 mag and an absolute Johnson B magnitude of -16.14 mag.

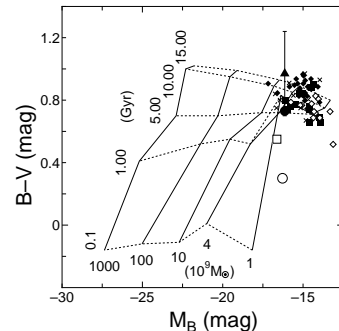


FIG. 3.— Absolute B -magnitude versus $B - V$ color diagram. Filled circle and filled triangle indicate TDSS. Open circle and open square indicate the tidal dwarf galaxies Arp 105S and Arp 245N, respectively. Filled squares, open diamonds, filled diamonds, and crosses represent dwarf elliptical galaxies in the Virgo cluster, Fornax cluster, Centaurus cluster, and NGC 5044 group, respectively. Solid lines and dotted lines represent the locus of chemo-photometric evolution models taken from Arimoto & Yoshii (1987): the galaxy mass of $M_G/10^9 M_\odot = 1, 4, 10, 100, \text{ and } 1000$, and the age $t = 0.1, 1, 5, 10, \text{ and } 15$ Gyr.

In Figure 3, we plot the data points for TDSS together with those of two tidal dwarf galaxies, Arp 105S ($V_{\text{GSR}} = 8518 \text{ km s}^{-1}$; de Vaucouleurs et al. 1991) and Arp 245N ($V_{\text{GSR}} = 2175 \text{ km s}^{-1}$, which is the average value of the V_{GSR} of NGC 2992 and NGC 2993; de Vaucouleurs et al. 1991; Braine et al. 2000), and dwarf ellipticals in the Virgo cluster (Bothun et al. 1989), the Fornax cluster (Bothun et al. 1989), the Centaurus cluster (Bothun et al. 1989), and the NGC 5044 group (Cellone 1999). We also show theoretical loci of chemo-photometric evolution models taken from Arimoto & Yoshii (1987). The $B - V$ and M_B properties of TDSS are different from those of Arp 105S ($M_B = -16.28$, $B - V = 0.3$) and Arp 245N ($M_B = -16.63$, $B - V = 0.55$) (Braine et al. 2000). In Figure 3 TDSS is located near the bright end of the loci of dwarf ellipticals in nearby clusters. Braine et al. (2000) suggested that Arp 105S and Arp 245N have experienced recent (< 1 Gyr) bursts of star formation. However, the data shown in Figure 3 suggests that a recent (< 1 Gyr) star formation burst has not occurred in TDSS.

Schombert et al. (1990) showed averaged the $B - V$ color of tidal features (tails, bridges, plumes, and envelopes) of 0.64 ± 0.24 . The $B - V$ color of TDSS is similar to or redder than those of these tidal features.

²SKYCAT is a tool that combines visualization of images and access to catalogs and archive data for astronomy provided by ESO. GAIA is an image display and analysis tool that adds many photometry related features to SKYCAT.

TABLE 1
PHOTOMETRIC PROPERTIES OF TDSS

Passband	λ_c^a (Å)	m_{obs}^b (mag)	A_λ^c (mag)	m_c^d (mag)	f_λ (ergs s ⁻¹ cm ⁻² Å ⁻¹)
<i>F336W</i> ^e	3317 ± 185	>17.85 ± 0.01	0.30	>17.56 ± 0.01	<3.45 ^{+0.04} _{-0.04} × 10 ⁻¹⁶
<i>F439W</i> ^e	4283 ± 232	16.80 ± 0.01	0.24	16.56 ± 0.01	8.62 ^{+0.05} _{-0.05} × 10 ⁻¹⁶
	4283 ± 232	16.77 ± 0.01	0.24	16.53 ± 0.01	8.84 ^{+0.06} _{-0.06} × 10 ⁻¹⁶
<i>F555W</i> ^e	5202 ± 611	16.59 ± 0.003	0.18	16.41 ± 0.003	9.94 ^{+0.03} _{-0.03} × 10 ⁻¹⁶
<i>V</i>	5505 ± 414	16.36 ± 0.27	0.18	16.17 ± 0.27	1.22 ^{+0.34} _{-0.27} × 10 ⁻¹⁵
<i>VR_{AB}</i>	5994 ± 998	16.05 ± 0.05	0.17 ^f	15.89 ± 0.05	1.34 ^{+0.06} _{-0.06} × 10 ⁻¹⁵
<i>R_c</i>	6588 ± 784	15.90 ± 0.04	0.15	15.76 ± 0.04	1.07 ^{+0.04} _{-0.04} × 10 ⁻¹⁵
<i>I_c</i>	8060 ± 771	15.24 ± 0.03	0.11	15.13 ± 0.03	9.86 ^{+0.29} _{-0.28} × 10 ⁻¹⁶
<i>F814W</i> ^e	8203 ± 879	16.67 ± 0.003	0.11	16.56 ± 0.003	8.63 ^{+0.02} _{-0.02} × 10 ⁻¹⁶
<i>J</i>	12500 ± 1055	14.17 ± 0.09	0.05	14.12 ± 0.09	7.55 ^{+0.65} _{-0.60} × 10 ⁻¹⁶
<i>H</i>	16500 ± 1490	13.52 ± 0.10	0.03	13.48 ± 0.10	4.65 ^{+0.45} _{-0.41} × 10 ⁻¹⁶
<i>K^g</i>	22200 ± 1950	13.13 ± 0.08	0.02	13.05 ± 0.08	2.35 ^{+0.18} _{-0.17} × 10 ⁻¹⁶

^aErrors indicate half value of the full width at half maximum for each filter band.

^bNot corrected for Galactic extinction.

^cTaken from NASA Extragalactic Database (NED). Assuming $A_B=0.237$ mag (Schlegel et al. 1998), $E(B - V)=0.055$ mag, and an $R_V=3.1$ extinction curve (Cardelli et al. 1989).

^dCorrected for Galactic extinction.

^eAdopted STScI magnitude system (Holtzman et al. 1995).

^fAdopted simple average of $A_V=0.182$ and $A_R =0.147$.

^gTranslated from K' magnitude (Wainscoat & Cowie 1992)

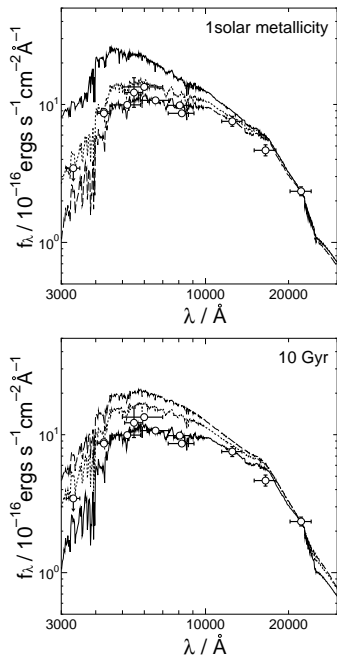


FIG. 4.— The spectral energy distribution of TDSS and simple stellar population models. Filled circles indicate the data for TDSS. Solid, dotted, and dashed lines indicate the simple stellar population model - (a) with solar metallicity at 1, 3, and 10 Gyr, and (b) the same model at 10 Gyr with 0.2 (dashed line), 0.4 (dotted line), and 1.0 (solid line) solar metallicity, respectively.

Next, we investigate the spectral energy distribution (SED) of TDSS. The observed SED is shown in Figure 4a. We also show model SEDs generated by GISEL96 (Bruzual & Charlot 1993; Charlot et al. 1996). Here we adopt the simple stellar population model with a Salpeter (1955) initial mass function (IMF), solar metallicity, and upper and lower mass cutoffs of $125 M_{\odot}$ and $0.1 M_{\odot}$, respectively. In Figure 4a, we show model SEDs with ages of 1 Gyr, 3 Gyr, and 10 Gyr. All the models have been scaled to the observed K' flux of TDSS for relative comparison to the observed SED. Furthermore we also show the results of a comparison of the 10 Gyr model SEDs with 0.2, 0.4, 1.0 solar metallicity to the observed SED in Figure 4b. These comparisons suggest that the observed SED is consistent with model SEDs of nearly solar metallicity with ages between 3 Gyr and 10 Gyr.

4. DISCUSSION

The main result from our multi-band photometric studies of the tidal debris in SS is that TDSS appears to consist of an old stellar population with > 0.4 solar metallicity (Figure 4a, 4b). Duc & Mirabel (1999) indicate that tidal dwarf galaxies have an average metallicity of one third of solar, which is independent of their absolute blue magnitude (Duc et al. 2000). The metallicity of TDSS thus appears to be higher with compared to tidal dwarf galaxies.

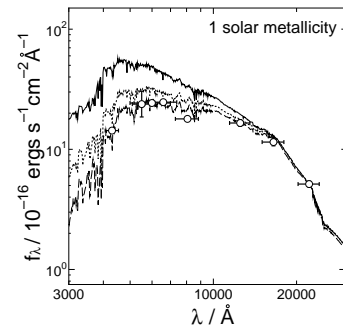


FIG. 5.— The spectral energy distribution of the outer part of HCG 79b and simple stellar population models. Filled circles indicate the data of HCG 79b. Solid, dotted, and dashed lines indicate the simple stellar population model with a solar metallicity at $t = 1, 3,$ and 10 Gyr, respectively.

The spatial configuration of TDSS and the member galaxies in SS and the spatial distribution of HI emission suggest that TDSS was liberated from HCG 79b during the strong interaction of HCG 79b with HCG 79d (Williams et al. 1991; Mendes de Oliveira & Hickson 1994). Therefore, it seems reasonable to consider that TDSS mainly consists of stars liberated from the outer region of HCG 79b. This means that the old stellar population with nearly solar metallicity in TDSS should be identical to that of the outer region of HCG 79b. In order to investigate the stellar population of the outer region of HCG 79b, we carried out aperture photometry of the outer region of HCG 79b by integrating the light within an annular ellipse with semi-major axes between $5''.2$ and $12''.0$. The lower cutoff radius is determined to avoid the inner star forming regions of HCG 79b (Vílchez & Iglesias-Páramo 1998; Shimada et al. 2000). The ellipse eccentricity and position angle are set to be 0.85 and 8° , respectively. The center coordinate of the annular ellipse is $\alpha = 15^{\text{h}}57^{\text{m}}00^{\text{s}}.8$, $\delta = +20^{\circ}54'15''.4$ (B1950.0) (Hickson 1993). In four *WFPC2* images, since lines of insensitive pixels run through the HCG79b, we cannot obtain the four fluxes (F_{336W} , F_{439W} , F_{555W} , F_{814W}) of TDSS with *WFPC2*. The resultant SED is shown in Figure 5 (see also Table 2). The same model SEDs used in Figure 4a are also shown in Figure 5. Although the I -band flux is a bit weaker than the model one, the overall SED is well described by a model SED with an age of 10 Gyr and solar metallicity. From these SED comparisons, it does seem likely that TDSS was liberated from HCG 79b by strong interaction with HCG 79d. This would then be the reason why the abundance of TDSS is richer than those of tidal dwarf galaxies. Schombert et al. (1990) has also shown that the colors of many tidal features are similar to the outer parts of the parent galaxies further strengthening the “stripping origin” hypothesis.

Comparing the spatial distribution of HI emission with the numerical simulation by Toomre & Toomre (1972), Williams et al (1991) suggested that the HI countertail and the optical counterarm from HCG 79b could have been generated ≈ 0.5 Gyr ago after the close encounter between HCG 79b and HCG 79d. Since it is known that tidal arms are promptly liberated from interacting galaxies, it seems likely that a secondary star formation event could have been induced during the early phase of tidal liberation such as appears to be the case in tidal dwarf galaxies (Figure 3).

TABLE 2
PHOTOMETRIC PROPERTIES OF THE OUTER PART OF HCG 79B

Passband	λ_c^a (Å)	m_{obs}^b (mag)	A_λ^c (mag)	m_c^d (mag)	f_λ (ergs s ⁻¹ cm ⁻² Å ⁻¹)
<i>F439W</i> ^e	4283 ± 232	16.28 ± 0.01	0.24	16.04 ± 0.01	$1.39_{-0.01}^{+0.01} \times 10^{-15}$
<i>V</i>	5505 ± 414	15.63 ± 0.27	0.18	15.45 ± 0.27	$2.38_{-0.52}^{+0.66} \times 10^{-15}$
<i>VR_{AB}</i>	5994 ± 998	15.41 ± 0.05	0.17 ^f	15.24 ± 0.05	$2.43_{-0.11}^{+0.12} \times 10^{-15}$
<i>R_c</i>	6588 ± 784	15.00 ± 0.04	0.15	14.85 ± 0.04	$2.47_{-0.08}^{+0.08} \times 10^{-15}$
<i>I_c</i>	8060 ± 771	14.58 ± 0.03	0.11	14.48 ± 0.03	$1.79_{-0.05}^{+0.05} \times 10^{-15}$
<i>J</i>	12500 ± 1055	13.31 ± 0.07	0.05	13.26 ± 0.07	$1.66_{-0.10}^{+0.11} \times 10^{-15}$
<i>H</i>	16500 ± 1490	12.53 ± 0.08	0.03	12.50 ± 0.08	$1.15_{-0.08}^{+0.09} \times 10^{-15}$
<i>K</i> ^g	22200 ± 1950	12.22 ± 0.06	0.02	12.20 ± 0.06	$5.14_{-0.28}^{+0.30} \times 10^{-16}$

^aErrors indicate half value of the full width at half maximum for each filter band.

^bNot corrected for Galactic extinction.

^cTaken from NASA Extragalactic Database (NED). Assuming $A_B=0.237$ mag (Schlegel et al. 1998), $E(B - V)=0.055$ mag, and an $R_V=3.1$ extinction curve (Cardelli et al. 1989).

^dCorrected for Galactic extinction.

^eAdopted STScI magnitude system (Holtzman et al. 1995).

^fAdopted simple average of $A_V=0.182$ and $A_R =0.147$.

^gTranslated from K' magnitude (Wainscoat & Cowie 1992)

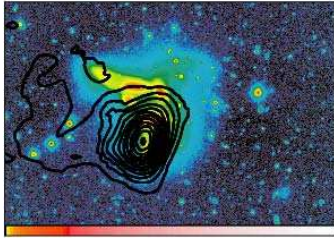


FIG. 6.— Optical $VR + I$ -band image and the intensity map of the HI emission taken from Williams et al. (1991). HI contours are drawn at levels 0.05, 0.15, 0.25, 0.35, 0.45, 0.55, 0.65, 0.75, 0.85, 0.95, 1.05, and $1.15 \text{ Jy km s}^{-1}$ per beam.

Williams et al. (1991) detected HI emission at a level of $1.4 \times 10^{20} \text{ H cm}^{-2}$ at the eastern end of TDSS. In Figure 6, we show our optical $VR + I$ image together with the HI intensity map taken from Williams et al. (1991). The HI emission appears associated with TDSS and distributed in an ellipse whose semi-major and semi-minor axes are $15''.0$ and $10''.0$, respectively. If we assume that the HI column density within this ellipse is constant at a value of $1.4 \times 10^{20} \text{ H cm}^{-2}$, we roughly estimate that the HI gas mass associated with TDSS is $2 \times 10^7 M_{\odot}$. Thus, we obtain a ratio of the HI gas mass to optical B -band luminosity of $3.2 \times 10^{-2} M_{\odot}/L_{\odot}$ for TDSS. This value is much smaller than those of Arp 105S ($L_B = 4.9 \times 10^8 L_{\odot}$, $M_{\text{HI}} = 4 \times 10^8 M_{\odot}$, $M_{\text{HI}}/L_B = 0.8 M_{\odot}/L_{\odot}$) and Arp 245N ($L_B = 6.1 \times 10^8 L_{\odot}$, $M_{\text{HI}} = 6 \times 10^8 M_{\odot}$, $M_{\text{HI}}/L_B = 1.0 M_{\odot}/L_{\odot}$). Furthermore, Vílchez & Iglesias-Páramo (1998) detect no $\text{H}\alpha$ emission in TDSS. This suggests the poverty of very massive stars in TDSS. These observations suggest that only a small amount of gas was involved in the formation of TDSS.

Bettoni & Fasano (1993) and Bonfanti et al. (1999) mentioned another possibility; i.e., TDSS (called “HCG 79b1” in their papers) is a pre-existing galaxy falling into SS that is being destroyed by galaxy-galaxy interaction. Since the photometric properties of TDSS are similar to those of dEs (i.e., $B-V$ colors and exponential surface brightness profiles), their idea may remain as a possible one. However, from the metallicity of TDSS, as determined from the SED, we suggest that TDSS is a tidally-induced object consisting primarily of stars liberated from HCG 79b. Further investigation of the mass-to-luminosity ratio and/or a more detailed investigation of the metallicity would be useful to confirm this hypothesis. It also requires numerical simulations to make sure whether tidally object being made by galaxy interactions without secondary star formation.

5. CONCLUSIONS

From multi-band photometry of the prominent tidal debris feature to the northeast of Seyfert’s Sextet we have obtained the following results:

1. The surface brightness profile of this tidal debris in Seyfert’s Sextet (TDSS) in each band shows an approximately exponential profile.
2. The observed $B - V$ color of TDSS is redder than those of tidal dwarf galaxies, e.g., Arp 105S and Arp 245N (Braine et al. 2000).
3. Comparing the spectral energy distribution (SED) of TDSS with theoretical photometric evolution models, we find that its SED is comparable to that of a stellar population with age ~ 10 Gyr and with higher metallicity than the average values found in tidal dwarf galaxies.
4. Comparing SEDs, we find that the SED of TDSS is similar to that of the stars in the outer part of HCG 79b.
5. TDSS seems to consist primarily of stars liberated from HCG 79b by strong galaxy interaction.

We conclude that TDSS is simply a passive tidal feature like many others in interacting galaxy systems. We also conclude that there is no indication that TDSS will evolve into a star-forming tidal dwarf galaxy similar to those previously studied. This, however, indicates that another type of forming dwarf galaxy without secondary star formation through the galaxy interaction.

We would like to thank the staff members of the Okayama Astrophysical Observatory, the KISO observatory and the UH 2.2 m telescope for their kind assistance during our observations. We thank J. W. Sulentic for his HST observation of Seyfert’s Sextet, and an anonymous referee for several useful comments which helped improve the paper. We also thank Ichi Tanaka for his kind help during our observations, Richard Wainscoat and Shinki Oyabu for their useful comments on photometric calibration, and Daisuke Kawata for useful discussions. A part of this work was done when YT was a visiting astronomer at the IfA, University of Hawaii. YT would like to thank Rolf-Peter Kudritzki and Bob McLaren for their warm hospitality. YS thanks the Japan Society for Promotion of Science (JSPS) Research Fellowships for Young Scientist. This work was supported in part by the Ministry of Education, Science, Sports and Culture in Japan under Grant Nos. 07055044, 10044052, and 10304013.

REFERENCES

- Arimoto, N. & Yoshii, Y. 1987, *A&A*, 173, 23
 Barnes, S. A., and Hernquist, L. 1992, *Nature*, 360, 715
 Bergvall, N., & Johansson, L. 1985, *A&A*, 149, 475
 Bettoni, D., & Fasano, G. 1993, *AJ*, 105, 1291
 Binggeli, B., Sandage, A., & Tammann, G. A. 1988, *ARA&A*, 26, 509
 Binggeli, B., Tarengi, M., & Sandage, A. 1990, *A&A*, 228, 42
 Bonfanti, P., Simien, F., Rampazzo, R., & Prugniel, Ph. 1999, *A&AS*, 139, 483
 Bothun, G. D., Caldwell, N., & Schombert, J. M. 1989, *AJ*, 98, 1542
 Braine, J., Lisenfeld, U., Due, P.-A., & Leon, S. 2000, *Nature*, 403, 867
 Bruzual, A. G., & Charlot, S. 1993, *ApJ*, 405, 538
 Cardelli, J. A., Clayton, G. C., & Mathis, J. S. 1989, *ApJ*, 345, 245
 Carpenter, J. M. 2001, *AJ*, 121, 2851
 Cellone, S. A. 1999, *A&A*, 345, 403
 Charlot, S., Worthey, G., & Alessandro, B. 1996, *ApJ*, 457, 625
 Dekel, A., & Silk, J. 1986, *ApJ*, 303, 39
 de Vaucouleurs, G., de Vaucouleurs, A., Corwin, H. G. Jr., Buta, R. J., Paturel, G., & Fouqué, P. 1991, *Third Reference Catalogue of Bright Galaxies* (Springer-Verlag)
 Dressler, A. 1980, *ApJ*, 236, 351

- Duc, P. -A. 1999, in IAU Symp. 186, Galaxy Interactions at Low and High Redshift, ed. Barnes, J. E., & Sanders, D. B. (Dordrecht: Kluwer), 61
- Duc, P. -A., & Mirabel, I. F. 1994, A&A, 289, 83
- Duc, P. -A., & Mirabel, I. F. 1998, A&A, 333, 813
- Duc, P. -A., Brinks, E., Springel, V., Pichardo, B., Weinbacher, P., & Mirabel, I. F. 2000, AJ, 120, 1238
- Elmegreen, B. G., Kaufman, M., & Thomasson, M. 1993, ApJ, 412, 90
- Faber, S. M., & Lin, D. M. C. 1983, ApJ, 266, L17
- Ferguson, H. C., & Binggeli, B. 1994, A&AR, 6, 67
- Frenk, C. S., Evrard, A. E., White, S. D. M., & Summers, F. J. 1996, ApJ, 472, 460
- Hamabe, M., & Ichikawa, S. 1992, in Proc. of Astronomical Data Analysis Software and Systems I, Astron. Soc. Pacific Conference Series, Vol. 25, eds. D. Worrall, Biemesderfer, and J. Barnes (ASP, San Francisco), 325
- Hickson, P. 1982, ApJ, 255, 382
- Hickson, P. 1993, Astrophys. Lett. & Comm., 29, 1
- Hickson, P., Mendes de Oliveira, C., Huchra, J. P., & Palumbo, G. G. C. 1992, ApJ, 399, 353
- Holtzman, J. A., Burrows, C. J., Casertano, S., Hester, J. J., Trauger, J. T., Watson, A. M., & Worthey, G. 1995, PASP, 107, 1065
- Huchtmeier, W. K. 1997, A&A, 325, 473
- Hunsberger, S. D., Charlton, J. C., & Zaritsky, D. 1997, ApJ, 462, 50
- Hunsberger, S. D., Charlton, J. C., & Zaritsky, D. 1998, ApJ, 505, 536
- Hunt, L. K., Mannucci, F. M., Testi, L., Migliorini, S., Stanga, R. M., Baffa, C., Lisi, F., & Vanzi, L. 1998, AJ, 115, 2594
- Ichikawa, S., Wakamatsu, K., & Okamura, S. 1986a, ApJS, 60, 475
- Ichikawa, S., Wakamatsu, K., & Okamura, S. 1986b, ApJS, 62, 253
- Itoh, N., Yanagisawa, K., & Ichikawa, T. 1995, Proc. SPIE, 2552, 430
- Jewitt, D., Luu, J., & Chen, J. 1996, AJ, 112, 1225
- Kauffmann, G., Nusser, A., & Steinmetz, M. 1997, MNRAS, 286, 795
- Kislyuk, V., Yatsenko, A., Ivanov, G., Pakuliak, L., & Sergeeva, T. 1999, The FON Astrogaphic Catalogue, Main Astronomical Observatory of National Academy of Science of Ukraine
- Kormendy, J. 1985, ApJ, 295, 73
- Landolt, A.U. 1992, AJ, 104, 340
- Larson, R. B. 1974, MNRAS, 166, 585
- Luppino, G., Metzger, M., Kaiser, N., Clowe, D., Gioia, I., & Mayazaki, S. 1996, in ASP Conf. Ser. 88, Clusters, Lensing, and the Future of the Universe, ed. V. Trimble & A. Reisenegger (San Francisco: ASP), 229
- Mateo, M. 1998, ARA&A, 36, 435
- Mendes de Oliveira, C., & Hickson, P. 1994, ApJ, 427, 684
- Mirabel, I. F., Lutz, D., & Maza, J. 1991, A&A, 243, 367
- Mirabel, I. F., Dottori, H., and Lutz, D. A&A, 1992, 256, L19
- Nishiura, S., Shimada, M., Ohyama, Y., Murayama, T., & Taniguchi, Y. 2000a, AJ, 120, 1691
- Nishiura, S., Muryama, T., Shimada, M., Sato, Y., Nagao, T., Molikawa, K., Taniguchi, Y. & Sanders, D. B. 2000b, AJ, 120, 2355
- Okazaki, T., & Taniguchi, Y. 2000, ApJ, 543, 149
- Rabaça, C. R. 1997, PhD thesis, The University of Alabama
- Rose, J. A. 1977, ApJ, 211, 311
- Rubin, V. C., Hunter, D. A., & Ford, W. K. Jr. 1991, ApJS, 76, 153
- Salpeter, E. E. 1955, ApJ, 121, 161
- Schlegel, D. J., Finkbeiner, D. P., & Davis, M. 1998, ApJ, 500, 525
- Schombert, J. M., Wallin, J. F., & Struck-Marcell, C. 1990, AJ, 99, 497
- Schweizer, F. 1978, in Structure and Properties of Nearby Galaxies, ed. Berkhuijsen, E. M. & Wieleinski, R. (Reidel, Dordrecht), 279
- Schweizer, F. 1982, ApJ, 252, 455
- Seyfert, C. K. 1948a, Phys. Rev., 74, 129
- Seyfert, C. K. 1948b, AJ, 53, 203
- Shakhbazyan, R. K. 1973, Astrofiz., 9, 495
- Shimada, M., Ohyama, Y., Nishiura, S., Murayama, T. & Taniguchi, Y. 2000, AJ, 119, 2664
- Sulentic, J. W., & Lorre, J. J. 1983, A&A, 120, 36
- Toomre, A., & Toomre, J. 1972, ApJ, 178, 623
- Urban, S. E., Corbin, T. E., & Wycoff, G. L. 1997, The Astrogaphic Catalogue on the Hipparcos System, US Naval Observatory
- Vader, J. P., & Sandage, A. 1991, ApJ, 379, L1
- Vílchez, J. M. & Iglesias-Páramo, J. 1998, ApJS, 117, 1
- Wainscoat, R. J., & Cowie, L. L. 1992, AJ, 103, 332
- Weilbacher, P. M., Duc, P.-A., Fritze von Alvensleben, U., Martin, P., & Fricke, K. J. 2000, A&A, 358, 819
- White, S. D. M., & Frenk, C. S. 1991, ApJ, 379, 52
- Williams, B. A., McMahon, P. M., & van Gorkom, J. H. 1991, AJ, 101, 1957
- Williams, B. A. & Rood, H. J. 1987, ApJS, 63, 265
- Wu, W., Rabaça, C. R., & Sulentic, J. W. 1994, AAS, 185, 106.02
- Yoshida, M., Taniguchi, Y., & Murayama, T. 1994, PASJ, 46, L195
- Zwicky, F. 1956, Multiple Galaxies, Ergebnisse Exakten Naturwissenschaften, 29, 344